Free-energy cost of localizing a single monomer of a confined polymer

James M. Polson and Zakary R. N. McLure
Department of Physics, University of Prince Edward Island, 550 University Avenue, Charlottetown, Prince Edward Island, C1A 4P3, Canada

(Received 1 May 2019; published 18 June 2019)

We describe a simple Monte Carlo simulation method to calculate the free-energy cost of localizing a single monomer of a polymer confined to a cavity. The localization position is chosen to be on the inside surface of the confining cavity. The method is applied to a freely jointed hard-sphere polymer chain confined to cavities of spherical and cubic geometries. In the latter case, we consider localization at a corner and at the center of a face of the confining cube. We consider cases of end-monomer localization both with and without tethering of the other end monomer to a point on the surface. We also examine localization of monomers at arbitrary positions along the contour of the polymer. We characterize the dependence of the free energy on the cavity size and shape, the localization position, and the polymer length. The quantitative trends can be understood using standard scaling arguments and use of a simple theoretical model. The results are relevant to those theories of polymer translocation that focus on the importance of the free-energy barrier as the translocation process requires an initial localization of a monomer to the position of a nanopore.

DOI: 10.1103/PhysRevE.99.062503

I. INTRODUCTION

The translocation of polymers through nanopores into, out of, or between enclosed spaces has been the subject of much theoretical interest for many years [1–10]. This work is driven in part by its relevance to various biological phenomena such as the packing and ejection of viral DNA (deoxyribonucleic acid) as well as the messenger RNA (ribonucleic acid) through the nuclear pore complex [11,12]. Another key motivation is for modeling the structural and dynamical behavior of polymers in randomly structured porous environments such as those composed of polymer networks and gels. In the so-called barrier-dominated regime, the chain dynamics are controlled by entropic trapping in and escape from cavitylike spaces separated by narrow constrictions. This behavior has also been studied in ordered media patterned with molecular-sized spatial constraints fabricated using colloidal templating [13]. Modeling such systems as a collection of spherical chambers separated by narrow cylindrical pores [9,10,14], computer simulations have revealed a rich variety of dynamical behavior that is governed largely by the relative size of the polymer and the chambers and the resulting spatial distribution of the polymer. If the chamber-to-polymer size ratio is small, the polymer may typically span several cavities, while for larger ratios the entire polymer resides in a single chamber and occasionally translocates wholly into a neighboring one. Another related simulation study [15] examined similar effects for translocation through a simple two-nanopore single-cavity structure whose design was motivated by previous experimental work [16]. More recently, Magill *et al.* extended this work and examined the translocation behavior of polymers in a sequential nanopore-channel device, which was proposed as a means to separate polymers by size [6].

Central to some theories of dynamics of polymers in porous media is the concept of an entropic barrier [1,17]. The passage of the polymer through a pore imposes spatial constraints that significantly reduce its conformational entropy and thus increase the free energy. Since the height of the barrier is the main determinant of the dynamical behavior in the barrier-dominated regime, its characterization with respect to the system properties is essential. There are two main contributions to the barrier. The first is the free-energy cost of localizing an end monomer to the location of a pore, and the second is determined by the variation of the free energy with respect to the degree of translocation during the so-called threading stage [17]. The second contribution has been extensively studied. Analytical approximations for the free-energy function were prominent in some of the earliest theoretical studies of translocation [2,18], and its main scaling properties have recently been characterized using Monte Carlo simulations [5,19].

The contribution to the free-energy barrier from end-monomer localization has received less attention. Analytical expressions for this free energy have been derived by Muthukumar and coworkers using the Green's function solution for a Gaussian chain under spherical confinement with and without tethering of an end monomer to the confining surface [3,4,10]. However, there have been no corresponding calculations using simulation methods carried out to test the accuracy of such analytical results. Two previously developed simulation techniques can in principle be used for this purpose. The first is that of Laachi and Dorfman, who introduced a Monte Carlo method to estimate the partition function (and therefore total free energy) of single- and double-tethered lattice-model polymers confined to a spherical cavity [7]. Another approach is the incremental gauge cell method developed by Rasmussen *et al.* [20], which was used to calculate the incremental chemical potential (and thus the total confinement free energy) of a chain tethered to the inner surface of a confining sphere [8]. The end-monomer localization free energy can be calculated as the difference between the free energies of

tethered and untethered polymers confined to a cavity, where the latter quantity can be calculated using a technique such as thermodynamic integration [21].

In this study, we describe a Monte Carlo simulation method to calculate the free-energy cost of localizing a single monomer to the inner surface of a confinement cavity. The method has several advantages over the two referenced above. First, it does not require a separate calculation of the confinement free energy of an untethered chain. In addition, the simulations do not require use of a lattice model, as in Ref. [7]. Like the approach in Ref. [7] and unlike that of Ref. [8], it can easily be used to determine the end-monomer localization free energy in the case where the other end monomer is tethered to a different position in the cavity. This feature is essential when using the results to understand the polymer dynamics in systems where the polymer spans several cavities [9,10,14]. Finally, our method can be used to calculate the free-energy cost of localizing *any* monomer for a polymer of *arbitrary* topology (e.g., linear, ring, branched). Such versatility enables calculations relevant, for example, to the translocation of a folded polymer, where the first monomer through the pore is not an end monomer [22].

We use the method to calculate the localization free energy for the simple but illustrative cases of a single linear polymer confined to a spherical and a cubic cavity. In the latter case, we consider end-monomer localization to both the center of one cube face and to a corner of the cube. We also examine localization for monomers at various locations along the chain contour, as well as the case of end-monomer localization for a chain with one tethered end. We show that the results are quantitatively consistent with known results in the limiting case of very weak confinement. Using a simple theoretical model, we also show that the scaling of the free energy with polymer length and cavity size and shape is semiquantitatively consistent with the expected trends.

The remainder of this article is organized as follows. In Sec. II, we present and justify the Monte Carlo (MC) algorithm for calculating the free energy. Section III provides a brief description of the model employed in the simulations, while Sec. IV provides the relevant details of the implementation of the algorithm in the simulation. Section V presents the simulation results for the various systems we have examined, as well as the predictions from theoretical models developed in the appendices. Finally, Sec. VI summarizes the main conclusions of this work.

II. DEVELOPMENT OF THE METHOD

In this section, we develop the Monte Carlo method used to calculate the free-energy cost of localizing a single monomer to a point on the inside surface of a cavity within which the polymer is confined. For convenience, we present the theoretical justification of the algorithm for the special case of localizing an end monomer in the absence of any constraints other than confinement to the cavity.

A. Free-energy cost of partial localization of chain end

We first describe a method to measure the free-energy difference between two polymer systems with difference degrees of confinement of a single end monomer. In one system, the end monomer is confined to a volume V_a', while the other is confined to a volume V_b', which is chosen to be a subvolume of V_a'. In addition, both V_a' and V_b' are subvolumes of the volume V of the cavity within which the entire polymer is confined.

Consider a freely jointed polymer chain of $N+1$ monomers with positions $\mathbf{r}_0, \mathbf{r}_1, \mathbf{r}_2, \ldots, \mathbf{r}_N$. We define the related set of $N+1$ vector coordinates $\mathbf{R}_n$ such that $\mathbf{R}_0 = \mathbf{r}_0$ and $\mathbf{R}_n = \mathbf{r}_n - \mathbf{r}_{n-1}$ for n ranging from 1 to N. Consider as well the case where the polymer is confined to a box of volume V and one end monomer is confined to a volume $V' < V$, where V' lies within the volume V. The potential energy of the polymer, $U(\mathbf{R}_0, \mathbf{R}_1, \ldots, \mathbf{R}_N; V') \equiv U(\mathbf{R}_0, \mathbf{R}^N; V')$, can be partitioned,

$$U = U_{\rm int}(\mathbf{R}^N) + U_{\rm ext}(\mathbf{R}_0, \mathbf{R}^N; V'), \tag{1}$$

where $U_{\rm int}(\mathbf{R}^N)$ is the internal potential energy associated with the interactions between bonded and nonbonded monomers, and $U_{\rm ext}(\mathbf{R}_0, \mathbf{R}^N; V')$ is the interaction between the monomers and the confining walls. The configurational partition function is given by

$$Z(V') = \int d^3\mathbf{R}_0 \int d^{3N}\mathbf{R} \exp[-\beta(U_{\rm int}(\mathbf{R}^N) + U_{\rm ext}(\mathbf{R}_0, \mathbf{R}^N; V'))], \tag{2}$$

and the configurational contribution to the free energy is

$$F(V') = -k_{\rm B}T \ln Z(V'), \tag{3}$$

where $k_{\rm B}$ is Boltzmann's constant and T is absolute temperature.

Now consider two systems, **a** and **b**, distinguished only by different containment volumes for the $n = 0$ monomer, V_a' and V_b'. The difference in the free energies for these states is

$$\Delta F \equiv F(V_b') - F(V_a') = -k_{\rm B}T \ln\left[\frac{Z(V_b')}{Z(V_a')}\right]. \tag{4}$$

Thus,

$$\beta\Delta F = -\ln\left[\frac{\int d^{3(N+1)}\mathbf{R} \exp[-\beta U_{\rm int}(\mathbf{R}^N)] \exp[-\beta U_{\rm ext}(\mathbf{R}^{N+1}; V_b')]}{\int d^{3(N+1)}\mathbf{R} \exp[-\beta U_{\rm int}(\mathbf{R}^N)] \exp[-\beta U_{\rm ext}(\mathbf{R}^{N+1}; V_a')]}\right],$$

where $\beta \equiv 1/k_B T$. Let the confinement volume for case **b** lie within the confinement volume for case **a**. Obviously, this also implies that $V_b < V_a$. In addition, it is clear that

$$\exp[-\beta U_{ext}(\mathbf{R}^{N+1}; V_b')] = \exp[-\beta(U_{ext}(\mathbf{R}^{N+1}; V_b') + U_{ext}(\mathbf{R}^{N+1}; V_a'))].$$

This follows from the fact that if the end monomer lies with V_b', where $U_{ext}(\mathbf{R}^{N+1}; V_b') = 0$, then it also lies within the volume V_a', where $U_{ext}(\mathbf{R}^{N+1}; V_a') = 0$. Likewise, if it lies outside V_b', then $U_{ext}(\mathbf{R}^{N+1}; V_b') = \infty$, regardless of whether it lies inside or outside of V_a'. Thus,

$$\beta \Delta F = -\ln\left[\frac{\int d^{3(N+1)}\mathbf{R} \exp[-\beta U_{ext}(\mathbf{R}^{N+1}; V_b')] \exp[-\beta U(\mathbf{R}^{N+1}; V_a')]}{\int d^{3(N+1)}\mathbf{R} \exp[-\beta U(\mathbf{R}^{N+1}; V_a')]}\right] \tag{5}$$

or

$$\beta \Delta F = -\ln\langle \exp[-\beta U_{ext}(\mathbf{R}^{N+1}; V_b')]\rangle_a, \tag{6}$$

where $\langle \cdots \rangle_a$ denotes an ensemble average using the potential $U(\mathbf{R}^{N+1}, V_a')$.

To estimate this free-energy difference in a MC simulation, the configurational states of the system are generated using the potential $U(\mathbf{R}^{N+1}, V_a')$. Thus, the end monomer is confined to the volume V_a' while the remaining monomers are confined to the volume V. The average is obtained by sampling the exponential in Eq. (6) using these configurations. The external potential energies of monomers labeled by $n = 1$ to N will always be zero, since these monomers always lie within the volume V. On the other hand, the external potential energy for the $n = 0$ monomer is $u_{ext}(\mathbf{R}_0) = 0$ if $\mathbf{R}_0$ is inside V_b' and $u_{ext}(\mathbf{R}_0) = \infty$, if $\mathbf{R}_0$ lies outside V_b'. Thus,

$$\begin{aligned} \exp[-\beta U_{ext}(\mathbf{R}^{N+1}; V_b')] &= 1, \quad \text{if } \mathbf{R}_0 \text{ inside } V_b' \\ &= 0, \quad \text{if } \mathbf{R}_0 \text{ outside } V_b'. \end{aligned} \tag{7}$$

If this quantity is sampled in a MC simulation M times and the mth sampling gives a value S_m, then the free-energy difference is then approximately

$$\beta \Delta F \approx -\ln\left[(1/M)\sum_{m=1}^{M} S_m\right]. \tag{8}$$

The approximation is expected to become exact in the limit $M \to \infty$.

B. Localization of the end monomer

We now show how the procedure described above in Sec. II A to measure the free-energy difference between systems of different degrees of confinement of the chain end can be used to measure the free-energy cost of localizing the end monomer to a point on the confinement surface. Returning to the configurational partition function of Eq. (2), we write

$$\begin{aligned} Z(V') = &\int d^{3N}\mathbf{R} \exp[-\beta U_{int}(\mathbf{R}^N)] \\ &\times \int d^3\mathbf{R}_0 \exp[-\beta U_{ext}(\mathbf{R}_0, \mathbf{R}^N; V')]. \end{aligned}$$

Defining the quantity

$$W_{ext}(\mathbf{R}^N, V') = -k_B T \ln \Omega(\mathbf{R}^N, V'),$$

where

$$V'\Omega(\mathbf{R}^N, V') \equiv \int d^3\mathbf{R}_0 \exp[-\beta U_{ext}(\mathbf{R}_0, \mathbf{R}^N; V')],$$

it follows

$$Z(V') = V' \int d^{3N}\mathbf{R} \exp[-\beta(U_{int}(\mathbf{R}^N) + W_{ext}(\mathbf{R}^N, V'))].$$

Next, we define the contribution from the internal energy to the configurational partition function

$$Z_{int}(V') \equiv \int d^{3N}\mathbf{R} \exp[-\beta(U_{int}(\mathbf{R}^N) + W_{ext}(\mathbf{R}^N, V'))],$$

from which it follows that

$$Z(V') = V' Z_{int}. \tag{9}$$

The configurational free energy is given by

$$F(V') = -k_B T \ln V' + F_{int}(V'),$$

where we have defined

$$F_{int}(V') \equiv -k_B T \ln Z_{int}(V').$$

The quantity $F_{int}(V')$ can be considered the conformational free energy for a polymer with an end monomer constrained to lie within V'. Clearly, the free-energy difference between systems with $V' = V_a'$ and $V' = V_b' < V_a'$ is

$$\begin{aligned} \Delta F &\equiv [F(V_b') - F(V_a')] \\ &= k_B T \ln[V_a'/V_b'] + F_{int}(V_b') - F_{int}(V_a'). \end{aligned} \tag{10}$$

Now consider the case where $V' \to \delta V$, i.e., the end-monomer confinement volume becomes very small. Choose its location to be any point inside V and call this point the origin, **0**. For a sufficiently small volume,

$$\begin{aligned} \delta V\, \Omega(\mathbf{R}^N, \delta V, \mathbf{0}) &= \int d^3\mathbf{R}_0 \exp[-\beta U_{ext}(\mathbf{R}_0, \mathbf{R}^N; V')] \\ &\approx \delta V \exp[-\beta U_{ext}(\mathbf{0}, \mathbf{R}^N)] \end{aligned}$$

and thus

$$\Omega(\mathbf{R}^N, \delta V, \mathbf{0}) \approx \exp[-\beta U_{ext}(\mathbf{0}, \mathbf{R}^N)],$$

where $U_{ext}(\mathbf{0}, \mathbf{R}^N)$ denotes the potential energy of confinement for the polymer with the $n = 0$ monomer tethered to the origin. The approximation becomes exact in the limit where $\delta V \to 0$. It follows that

$$W_{ext}(\mathbf{R}^N, \delta V) \approx U_{ext}(\mathbf{0}, \mathbf{R}^N),$$

and thus Eq. (9) becomes

$$Z(\delta V) \approx \delta V \int d^{3N}\mathbf{R} \exp[-\beta(U_{int}(\mathbf{R}^N) + U_{ext}(\mathbf{0}, \mathbf{R}^N))].$$

This can be written

$$Z(\delta V) \approx \delta V Z_{\rm int}^{(0)},$$

where

$$Z_{\rm int}^{(0)} \equiv \int d^{3N}\mathbf{R} \exp[-\beta(U_{\rm int}(\mathbf{R}^N) + U_{\rm ext}(\mathbf{0}, \mathbf{R}^N))]$$

is the configurational partition function for a polymer confined and end tethered to a point inside V. Thus, for small δV, $Z_{\rm int}(\delta V) \approx Z_{\rm int}^{(0)}$. Consequently, the configurational free energy satisfies

$$F(\delta V) \equiv -kT_{\rm B} \ln \delta V + F_{\rm int}(\delta V) \approx -k_{\rm B}T \ln \delta V + F_{\rm int}^{(0)},$$

where

$$F_{\rm int}^{(0)} \equiv -k_{\rm B}T \ln Z_{\rm int}^{(0)}$$

is the configurational free energy for a case of a polymer tethered at the origin. Denoting the difference in the configurational free energy for systems with $V' = V$ and $V' = \delta V$ as

$$\Delta F(\delta V) \equiv F(\delta V) - F(V),$$

it follows that

$$\Delta F(\delta V) = k_{\rm B}T \ln(V/\delta V) + \Delta F_{\rm int}(\delta V), \tag{11}$$

where

$$\Delta F_{\rm int}(\delta V) \equiv F_{\rm int}(\delta V) - F_{\rm int}(V)$$

is approximately

$$\Delta F_{\rm int}(\delta V) \approx F_{\rm int}^{(0)} - F_{\rm int}(V).$$

This approximation becomes exact in the limit $\delta V \to 0$. We define $\Delta F_{\rm loc}$ as follows:

$$\begin{aligned}\Delta F_{\rm loc} &\equiv \lim_{\delta V \to 0} \Delta F_{\rm int}(\delta V) \\ &= \lim_{\delta V \to 0} [\Delta F(\delta V) - k_{\rm B}T \ln(V/\delta V)],\end{aligned} \tag{12}$$

where the difference is expected to converge in the limit. We identify $\Delta F_{\rm loc}$ as the chain-end localization free energy. This is the central quantity of this study.

The physical meaning of the quantity $\Delta F_{\rm loc}$ is as follows. Let $\mathcal{P}(V')$ be the probability that the end monomer lies in the subvolume V', where $0 < V' \leqslant V$. If we choose $V' = \delta V$ and $V' = V$ and note that $\mathcal{P}(V) = 1$, it is clear that

$$\mathcal{P}(\delta V) = \frac{\mathcal{P}(\delta V)}{\mathcal{P}(V)} = \frac{\exp[-\beta F(\delta V)]}{\exp[-\beta F(V)]}. \tag{13}$$

Using Eqs. (11) and (12), it is easily shown that

$$\mathcal{P}(\delta V) = \left(\frac{\delta V}{V}\right) \exp[-\beta \Delta F_{\rm loc}] \tag{14}$$

for an infinitesimal volume δV. The volume ratio prefactor is the probability that a single isolated particle lies inside δV in the absence of other monomers. The Boltzmann factor containing $\Delta F_{\rm loc}$ is the factor by which this probability is altered by virtue of the connection of the end monomer to the rest of the polymer. The case $\Delta F_{\rm loc} > 0$ corresponds to a probability depletion relative to the isolated-particle case, while $\Delta F_{\rm loc} < 0$ corresponds to an enhancement in the probability.

In principle, we can calculate $\Delta F_{\rm loc}$ by carrying out a simulation using the procedure outlined in Sec. II A to measure ΔF for a small but finite volume δV. However, for large $V/\delta V$, the statistics are expected to be poor. To circumvent this problem, we carry out a series of simulations employing a sequence of ever-decreasing values of V'. Equation (10) can be used to calculate the free-energy difference for systems of different monomer confinement volumes and the differences summed to obtain the chain-end localization free energy. As an example, consider the free-energy difference between systems with $V'_{\rm a} = V$ and $V'_{\rm b} = V/2$. From Eq. (10), it follows that

$$F(V/2) - F(V) = k_{\rm B}T \ln 2 + F_{\rm int}(V/2) - F_{\rm int}(V)$$

or

$$F_{\rm int}(V/2) - F_{\rm int}(V) = \Delta F_1 - k_{\rm B}T \ln 2,$$

where we define $\Delta F_1 \equiv F(V/2) - F(V)$. We can likewise find comparable expressions choosing $V'_{\rm a} = V/2$ and $V'_{\rm b} = V/4$, and then $V'_{\rm a} = V/4$ and $V'_{\rm b} = V/8$, and so on. Using those results, it is easily shown that

$$F_{\rm int}(V/2^n) - F_{\rm int}(V) = \sum_{m=1}^{n} \Delta F_m - nk_{\rm B}T \ln 2, \tag{15}$$

where

$$\Delta F_m \equiv F(V/2^m) - F(V/2^{m-1}). \tag{16}$$

Now, for sufficiently large n, $\delta V_n = V/2^n$ will be small enough to satisfy the previous approximations. Thus,

$$F_{\rm int}(V/2^n) - F_{\rm int}(V) \approx \Delta F_{\rm loc} \tag{17}$$

or

$$\Delta F_{\rm loc} \approx \sum_{m=1}^{n} (\Delta F_m - k_{\rm B}T \ln 2), \tag{18}$$

where the approximation becomes more accurate as n increases.

These results can be generalized by considering the case where the sequence of decreasing end-monomer confinement volumes is not generated by subsequent divisions by a factor of 2. Instead, we choose arbitrary ratios between successive subvolumes in the sequence. In this case, it can be shown that Eq. (16) should be modified to

$$\Delta F_m \equiv F(V_m) - F(V_{m-1}), \tag{19}$$

where

$$V_m \equiv \alpha_m V_{m-1} = \left(\prod_{i=1}^{m} \alpha_i\right) V, \tag{20}$$

and where the set of proportionality constants $\{\alpha_m\}_{m=1}^n$ are arbitrary. In addition, Eq. (18) should be modified to be

$$\Delta F_{\rm loc} \approx \sum_{m=1}^{n} \left(\Delta F_m - k_{\rm B}T \ln \alpha_m^{-1}\right). \tag{21}$$

In practice, the constants $\{\alpha_m\}_{m=1}^n$ should be chosen in a manner to optimize the statistical efficiency of the simulations. Note that the choice $\alpha_m = \frac{1}{2}$ reduces Eq. (19) to Eq. (16) and Eq. (21) to Eq. (18).

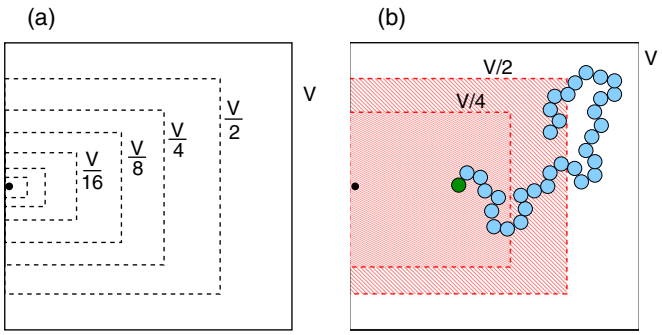

FIG. 1. Schematic illustration of the method used to calculate the chain-end localization free energy for volume subdivision fraction $\alpha_m = \frac{1}{2}$. (a) The volume subdivisions used to localize the chain end to a point (labeled as a black dot). Each successive subvolume is half of the previous subvolume in the sequence. (b) Illustration of method for calculating ΔF_m for $m = 2$. The center of the selected end monomer (colored green) is confined to lie within the volume $V/2$ (shaded red), while the centers of the remaining monomers (colored blue) can be anywhere in the full volume V. ΔF_2 is determined in a MC simulation by calculating the fraction of monomer center positions of the end monomer that lie within the volume $V/4$ (double-shaded red). Note that the localization point lies on the surface enclosing the volume accessible to the monomer *centers*. Thus, the subvolumes can be made arbitrarily small regardless of the finite size of the monomers.

To summarize the procedure formulated in this section, we can use the method described in Sec. II A, to measure the difference in the conformational free energy ΔF_m in Eq. (19) for successive reductions in the end-monomer confinement volume. These values are used in Eq. (21) to estimate the change in the internal conformational free energy of the polymer upon localization of the end monomer to a target location inside the cavity. As n (the number of subdivisions of the end-monomer confinement volume) increases, the estimate for $\Delta F_{\rm loc}$ in Eq. (21) is expected to converge to the correct value. Figure 1 provides a schematic illustration of the method used to calculate ΔF_m used in Eq. (16).

Note we have presented the development of the method assuming (1) end-monomer localization and (2) no other constraints (other than cavity confinement) are present. However, it is easily shown that the method is equally valid for localizing a monomer located at arbitrary position along the polymer contour or the case of monomer localization for a polymer with one end already tethered to a different point on the surface. Both of these other cases are also examined in this study.

III. MODEL

We model the polymer as a freely jointed chain of hard spheres, each with diameter σ. Pairs of bonded monomers interact with a potential $u_{\rm b}(r) = 0$ if $\sigma < r < 1.15\sigma$ and $u_{\rm b}(r) = \infty$, otherwise. The pair potential for nonbonded monomers is thus $u_{\rm nb}(r) = \infty$ for $r \leqslant \sigma$ and $u_{\rm nb}(r) = 0$ for $r > \sigma$, where r is the distance between the centers of the monomers. In a few calculations, we also examine the case where $u_{\rm nb} = 0$ for all values of r (i.e., no excluded volume interaction to prevent overlap of monomers). We refer to these model chains as "ideal" to distinguish them from the "real" chains in which the excluded volume interaction is present.

The polymer is confined to a cavity that is either cubic or spherical in shape. The cavity walls are "hard," such that the monomer-wall potential energy is $u_{\rm wall} = \infty$ if the monomer center lies with a distance of $\sigma/2$ from the nearest point on the wall, and $u_{\rm wall} = 0$ otherwise. The width of the cavity D is defined $D \equiv V^{1/3}$, where V is the volume of the box accessible to the monomer centers. Thus, $D = D_{\rm true} - \sigma$ for a cubic cavity with an actual width of $D_{\rm true}$, and $D = (\pi/6)^{1/3}(D_{\rm true} - \sigma)$ for a spherical cavity of actual diameter $D_{\rm true}$. The subvolumes for end-monomer confinement used in the localization algorithm were chosen to be hard-walled cavities of the same shape as the true confinement cavity. Thus, cubic subvolumes were used for cubic cavities and spherical subvolumes for spherical cavities.

IV. SIMULATION DETAILS

We employ the Metropolis Monte Carlo method to generate the states of the confined polymer system, where a state is defined by the collection of monomer coordinates. In most of the simulations, we calculate the localization free energy of an end monomer, though we also consider the case of localizing a monomer at arbitrary position along the polymer. Since the model system, including the artificial potentials imposed on the selected monomer, is athermal in character, trial moves are rejected if the move results in overlap of a monomer with another monomer or the wall, or if it violates the constraints associated with the bonds or localized-monomer confinement; otherwise, it is accepted with 100% probability. Trial moves are generated using a combination of random monomer displacement moves, crankshaft moves, reptation, and sequence-inversion moves. A sequence-inversion move is defined by the monomer coordinate exchange $\mathbf{r}_i \rightarrow \mathbf{r}_{N-i}$. Such moves do not change the shape or position of the polymer as a whole but do change the position of the monomer to be localized. In the case of end-monomer localization, the large end-monomer displacements that are produced are accepted with reasonably high probability only for the larger subvolumes in the earlier stages of the calculation, i.e., for lower values of the index m in Eq. (20). For smaller subvolumes, the acceptance ratio approaches zero and the moves are not used. In some simulations, we localize the end monomer of a polymer whose other end is already tethered to a point on the confining surface. In those cases, we cannot use reptation or sequence inversion moves.

Note the localization point is situated on the surface surrounding the volume accessible to monomer centers. Thus, it is located a distance of $\sigma/2$ away from the nearest point on the actual confinement surface. In addition, all subvolumes also refer to regions accessible to the center of the selected monomer. Consequently, the subvolumes can be made arbitrarily small, as required by the method, and are not limited by the monomer size. The number of volume subdivisions n used to calculate the localization free energy was chosen to be between $n = 12$ and $n = 30$, where large n was used for larger cavity sizes. The final subvolume was chosen to be $V_n/\sigma^3 = 0.02^3$, which fixes the values of the volume scaling constants α_m appearing in Eq. (20). For example, for a $D = 30$

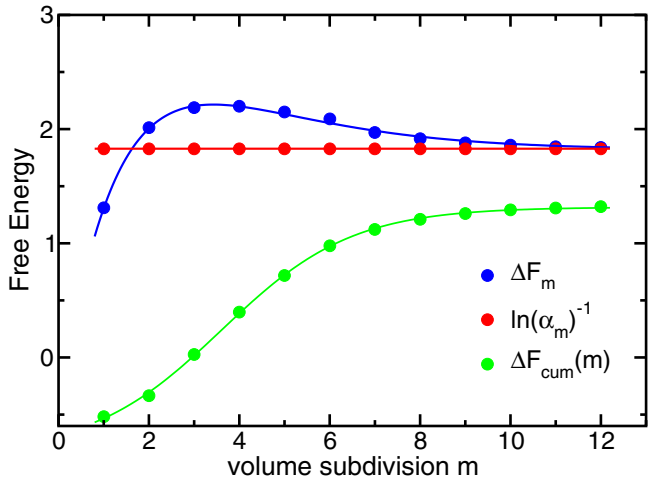

FIG. 2. Illustration of the convergence of the summation of Eq. (21) for the case of confinement in a cubic cavity of side length $D = 30$ and a polymer of length $N = 100$. Here, the volume subdivision ratio is $\alpha_m = 0.16069$ for the mth subdivision. ΔF_m represents the free-energy difference between localizing the end-monomer volumes V_m and V_{m-1}, where these subvolumes are defined in Eq. (20). In addition, $\ln(\alpha_m^{-1})$ is the free-energy difference (in units of k_BT) for a single isolated particle for confinement in these two subvolumes. These two quantities appear on the right side of Eq. (21). $\Delta F_{\rm cum}(m)$ is the cumulative sum of the difference in these two quantities. As the number of volume subdivisions m increases, $\Delta F_{\rm cum}(m)$ converges to $\Delta F_{\rm loc}$.

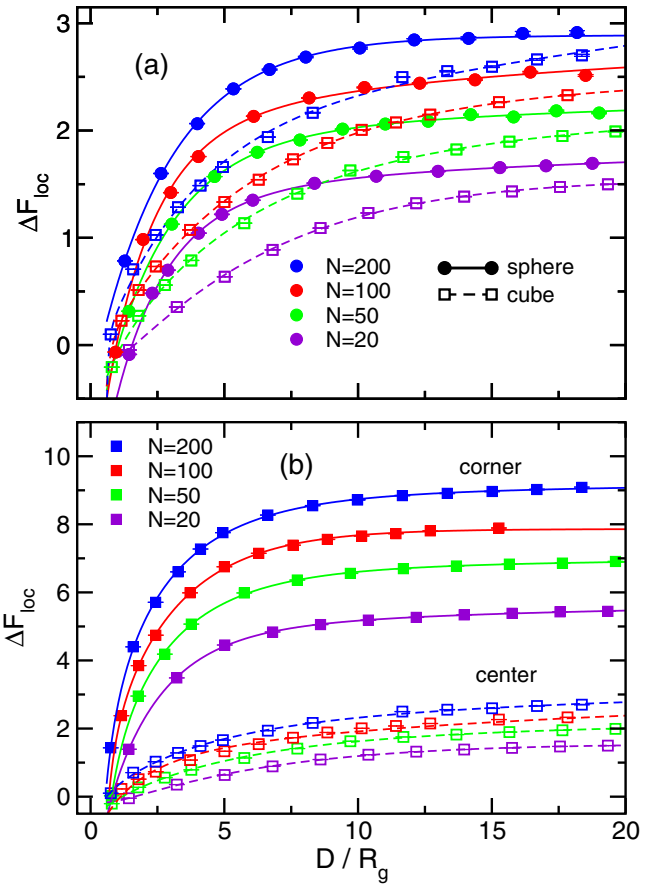

FIG. 3. (a) $\Delta F_{\rm loc}$ vs confining D/R_g for chains of length $N = 20$, 50, 100, and 200. Results are shown for both spherical cavities (solid circles) and cubic confinement cavities (open squares). For the cubic cavities, chain end localization occurs at the center of one side of the cube. Here, $D \equiv V^{1/3}$, where V is the volume of the confining cavity accessible to the monomer centers, and R_g is the radius of gyration of an unconfined polymer. (b) As in panel (a), except results are shown for localization of a chain end to the corner of a cube (solid squares) and the center of one face of a cube (open squares).

cubic cavity used for a $N = 100$ polymer, using $n = 12$ leads to $\alpha_m = 0.16069$ for all m.

At each stage of the calculation for a given end-monomer subvolume, the polymer was first equilibrated, following which a production run was used to acquire the data. As an example, for a simulation with a $N = 200$ polymer in a cubic cavity of width $D = 50$, the system was equilibrated for 5×10^6 MC cycles, following which a production of 1×10^8 MC cycles was carried out. A single-monomer move (translation or crankshaft), a reptation move, and an inversion move are each attempted on average once during each MC cycle. Maximum displacements for the single-monomer translational and crankshaft moves were chosen to yield acceptance ratios near 50%. Each free-energy calculation was performed between 5 and 10 times using different random number sequences. The statistically independent results were then used in the estimation of the standard error.

In the results presented below, distances are measured in units of σ and energy is measured in units of k_BT.

V. RESULTS

A. End-monomer localization

Figure 2 presents simulation results that illustrate the convergence of the summation of Eq. (21). For this case, the end monomer of a $N = 100$ polymer is localized to a point in the middle of one face of a confining cube of dimension $D = 30$. The graph shows ΔF_m vs m, where ΔF_m is the free-energy difference between localizing the end-monomer volumes V_m and V_{m-1}, where the subvolumes are defined in Eq. (20). In addition, the volume subdivision index ranges from $m = 1$ to $m = 12$. Also shown is the cumulative summation $\Delta F_{\rm cum}(m) \equiv \sum_{i=1}^{m}(\Delta F_i - \ln \alpha_i^{-1})$. As the number of volume subdivisions increases and thus the localization volume of the end monomer becomes very small, ΔF_m converges to $\ln \alpha_m^{-1}$. This indicates that any further reduction in the end-monomer confinement volume results simply in the reduction in translational entropy of that monomer and not to any change to the conformational free energy of the polymer. Thus, the value of the cumulative value $\Delta F_{\rm cum}(m)$ levels off to the localization free energy, $\Delta F_{\rm loc}$.

Figure 3 shows the localization free energy $\Delta F_{\rm loc}$ as a function of D/R_g, the confinement cavity size scaled by the radius of gyration of a free polymer, R_g. Results for polymer lengths of $N = 20$, 50, 100, and 200 are shown. Figure 3(a) shows free energies for end-monomer localization to a point on the surface of a confining sphere (solid symbols and lines) and for localization the midpoint of one face for confinement in a cubic cavity (open symbols and dashed lines). Figure 3(b) compares two sets of results for cubic confinement: one for

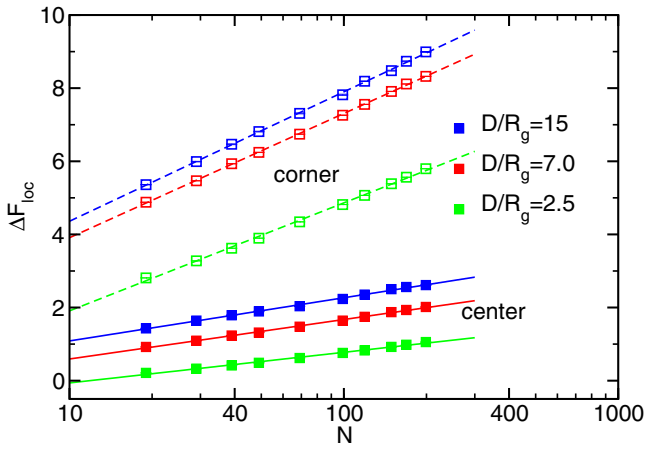

FIG. 4. (a) $\Delta F_{\rm loc}$ vs polymer length N for polymers confined to a cubic space. Results are shown for various ratios of $D/R_{\rm g}$ for the cases of chain-end localization to the center of one face of the cube (closed squares) and to one corner of the cube (open squares). The curves overlaid on the data are fits to $\Delta F_{\rm loc} = c + \alpha \ln N$. The fitting parameter values are as follows for localization to a corner: $\alpha = 1.54 \pm 0.01$ and $c = 0.82 \pm 0.06$ for $D/R_{\rm g} = 15$; $\alpha = 1.48 \pm 0.01$ and $c = 0.51 \pm 0.05$ for $D/R_{\rm g} = 7.5$; $\alpha = 1.28 \pm 0.02$ and $c = -1.04 \pm 0.08$ for $D/R_{\rm g} = 2.5$. For localization to the center of a face, the values are $\alpha = 0.51 \pm 0.01$ and $c = -0.09 \pm 0.04$ for $D/R_{\rm g} = 15$; $\alpha = 0.47 \pm 0.01$ and $c = -0.49 \pm 0.04$ for $D/R_{\rm g} = 7.5$; $\alpha = 0.36 \pm 0.01$ and $c = -0.90 \pm 0.04$ for $D/R_{\rm g} = 2.5$.

localization to a midpoint on a face (open symbols and dashed lines) and the other for localization to a corner of the cube (closed symbols and solid lines). The curves for each data set are shown as guides for the eye and are not fits using any theoretical prediction. In general, the free energy increases monotonically with cavity size and gradually levels off to some asymptotic value. $\Delta F_{\rm loc}$ rises rapidly with $D/R_{\rm g}$ for $D/R_{\rm g} \lesssim 5$ and is nearly constant for $D/R_{\rm g} \gtrsim 10$. For $D/R_{\rm g} \lesssim 1$, $\Delta F_{\rm loc}$ is even slightly negative. Thus, for a very tightly confined polymer, the end monomer has a higher probability of being at the point on a wall than would be the case for the monomer in the absence of the remaining portion of the polymer. We also note that $\Delta F_{\rm loc}$ is generally higher for spherical confinement compared to cubic confinement (with midface localization), though the two sets of results appear to converge to the same value as the confinement volume becomes very large. On the other hand, in the case of cubic confinement, the free energy for localization to a corner is consistently larger than that for the midface localization, even in the limit of very large confinement volumes. Finally, we note that in all cases $\Delta F_{\rm loc}$ increases monotonically with polymer length.

Figure 4 shows the variation of $\Delta F_{\rm loc}$ with polymer length for three different cavity sizes. In each case, results are shown for chain localization at the center of one face of the confining cube and at one corner of the sphere. As is evident in the figure, $\Delta F_{\rm loc}$ varies approximately linearly with $\ln N$. In addition, $\Delta F_{\rm loc}$ increases more rapidly with polymer length for end-monomer localization at a corner than for the case of localization near a cube face center. Consistent with the results of Fig. 3, the free energy increases with increasing confinement volume in all cases.

Each of the trends evident in Figs. 3 and 4 can be accounted for using standard scaling arguments together with simple theoretical modeling. Let us first consider the origin of the scaling of $\Delta F_{\rm loc}$ with N for the case of a very weakly confined polymer where $D/R_{\rm g} \gg 1$. It is useful to first note that in a scalefree environment the conformational contribution to the partition function of a self-avoiding chain can be written

$$Z_i = q^N N^{\gamma_i - 1}, \tag{22}$$

where N is the number of bonds of a polymer composed of $N+1$ monomers and $q = e^{-\mu/k_{\rm B}T}$, where μ is the chemical potential per monomer of the chain. In addition, γ_i is a critical exponent whose value depends on whether the polymer is free or tethered to a surface. For a free polymer ($i = {\rm a}$), $\gamma_a \approx 1.16$, while for a polymer tethered to an infinite flat surface ($i = {\rm b}$), $\gamma_{\rm b} \approx 0.69$ [17]. Since the free energy of a polymer is given by $F_i/k_{\rm B}T = -\ln Z_i$, it follows that the conformational free-energy difference between a free polymer and one tethered to a surface is $\Delta F_{\rm ab} \equiv F_{\rm b} - F_{\rm a} = \alpha_{\rm ab} \ln N$, where $\alpha_{\rm ab} \equiv \gamma_{\rm a} - \gamma_{\rm b} \approx 0.47$. Clearly, $\Delta F_{\rm ab}$ is equal to $\Delta F_{\rm loc}$ for chain-end localization to the center of a cubic box in the limit of infinite box size. For the largest confining cube we consider of $D/R_{\rm g} = 15$, a fit to the data yields $\alpha = 0.51 \pm 0.01$, which is comparable to though slightly larger than the theoretical prediction.

Now consider the case of a polymer tethered to the corner of an semi-infinite octant of space (e.g., the polymer is tethered at the origin and the polymer is constrained to lie in the region $x > 0$, $y > 0$, and $z > 0$). We label the index in Eq. (22) $i = {\rm c}$ for this case. The conformational free-energy difference between this tethered polymer and a free polymer is $\Delta F_{\rm ac} \equiv F_{\rm c} - F_{\rm a} = \alpha_{\rm ac} \ln N$, where $\alpha_{\rm ac} \equiv \gamma_{\rm c} - \gamma_{\rm a}$. This is the predicted form of $\Delta F_{\rm loc}$ for end-monomer localization at the corner of a confining cube in the limit of infinite cube size. For the largest confining cube we use (i.e., $D/R_{\rm g} = 15$), a fit to the data yields $\alpha = 1.51 \pm 0.02$. We are unaware of whether the scaling exponent $\gamma_{\rm c}$ has been calculated for such a corner-tethered polymer. Consequently, we have used a different Monte Carlo simulation method to measure the free energies $F_{\rm a}$, $F_{\rm b}$, and $F_{\rm c}$. The results are presented in Appendix A. We find that the length dependence of the polymer satisfies the relation

$$\Delta F_{\lambda\mu} = C_{\lambda\mu} + \alpha_{\lambda\mu} \ln N. \tag{23}$$

The quantity of interest here was found to be $\alpha_{\rm ac} = 1.451 \pm 0.001$, which compares well to the value for the data for the largest confining cube in Fig. 4.

The arguments above hold for large box size, i.e., $D/R_{\rm g} \gg 1$. In order to account for the variation of $\Delta F_{\rm loc}$ with box size, i.e., the localization free energy decreases with decreasing D, we develop a simple theoretical model based on the following simplifications. If the polymer end lies in a layer of width $\approx R_{\rm g}$ near the walls of the box, the polymer will interact with the box, leading to an increase in the conformational free energy. If the end monomer lies a distance $\gtrsim R_{\rm g}$ away from the walls of the box, the polymer does not interact with the walls and its conformational free energy, $F_{\rm a}$, is otherwise independent of position. Figure 12 in Appendix B shows

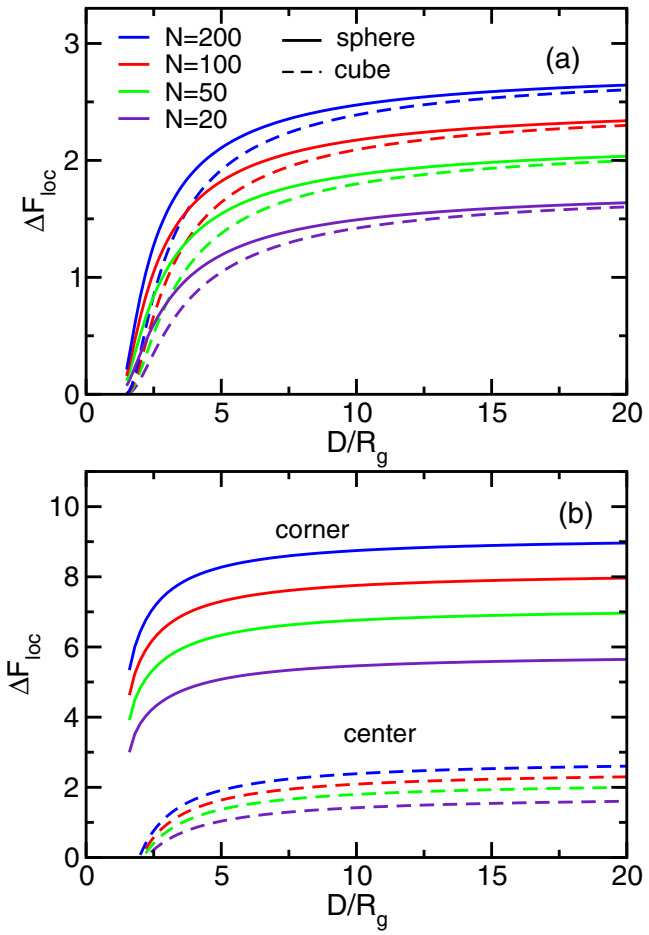

FIG. 5. Predictions for $\Delta F_{\rm loc}$ using the theoretical model of Appendix C. (a) $\Delta F_{\rm loc}$ vs $D/R_{\rm g}$ for $N = 20$, 50, 100, and 200. In each case, results are shown for end-monomer localization to the center of one face of the cubic box and to a point on the wall of a confining sphere. (b) As in panel (a), except results are shown for end-monomer localization to the center of one face of the cubic box and localization to one corner of the cube.

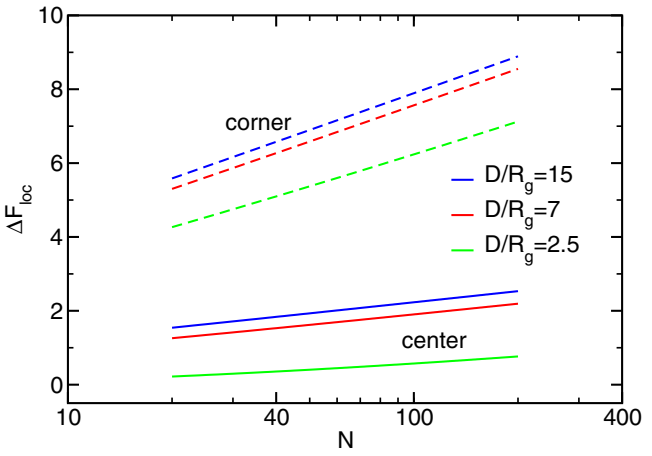

FIG. 6. Predictions for $\Delta F_{\rm loc}$ using the theoretical model of Appendix C. $\Delta F_{\rm loc}$ vs N for $D/R_{\rm g} = 2.5$, 7, and 15. In each case, results are shown for end-monomer localization to the center of one face of the cubic box and localization to one corner of the cube.

simulation results for the variation of the free energy with end-monomer position with distance from a wall for a variety of chain lengths and confirms this expected trend. For simplicity, we model the surface effects on the free energy by choosing a constant value when the chain end lies in a region close to the confining surface. The value of this free energy is chosen to be that calculated in Appendix A for a polymer tethered to a wall or corner. The theoretical model is developed in Appendix C. The localization free energy is calculated using Eqs. (C5)–(C7) for localization to the midpoint on a cubic face, Eqs. (C6), (C7), and (C9) for corner localization inside a cube and Eqs. (C6), (C10), and (C11) for localization to a point on the inside wall of a spherical cavity.

Figure 5(a) shows the prediction for the variation of $\Delta F_{\rm loc}$ with box size for several different polymer lengths. Results are shown for spherical and cubic box confinement with end-monomer localization to the center of one face of the confining cube and to one point on the confining sphere. Likewise, Fig. 5(b) compares results for $\Delta F_{\rm loc}$ for cubic confinement with end-monomer localization to the center of one face of the confining cube and localization to one of its corners. Figure 6 shows predicted variation of $\Delta F_{\rm loc}$ with polymer length for three different cubic box sizes. Results are shown for localization to both the center of one face and to one corner of the confining cube. The model correctly predicts the main qualitative trends, including (1) the rapid decrease in $\Delta F_{\rm loc}$ with decreasing cavity size for $D/R_{\rm g} \lesssim 4$; (2) the higher value of the free energy for localization to a corner vs the center of a face of the confining cube; (3) the consistently higher value of $\Delta F_{\rm loc}$ for confinement in a sphere compared to a cube of the same volume (with face-centered tethering); and (4) the linear variation of $\Delta F_{\rm loc}$ with $\ln N$ with approximately the same scaling factor. The quantitative discrepancies naturally arise from the approximations we have employed, notably choosing the conformational free energy to be constant within a finite range of end-monomer distance from the confining surface. However, the semiquantitative agreement demonstrates that our basic interpretation of the trends is correct.

B. Localization of arbitrary monomer

Thus far, we have examined the free energy of localizing a single end monomer to a point on the inside wall of a confining cavity. Consider now the case of localization of a monomer at arbitrary position along the contour of the polymer. We denote the index for this monomer $m_{\rm loc}$, which ranges from 0 to N for a polymer of $N+1$ monomers. Figure 7(a) shows the variation of $\Delta F_{\rm loc}$ with $m_{\rm loc}$ for a polymer of length $N = 200$. Note that in the figure $m_{\rm loc}$ is varied from from the position of one end monomer ($m_{\rm loc} = 0$) to the middle monomer ($m_{\rm loc} = 100$); the free energy for the range $m_{\rm loc} = 100$ to 200 is related by symmetry. Results are shown for two different cavity sizes. In each case, $\Delta F_{\rm loc}$ is smallest at the end position and increases rapidly with $m_{\rm loc}$ until about $m_{\rm loc} \approx 20$, after which it increases at a much slower rate. The free-energy maximum lies at $m_{\rm loc} = N/2 = 100$, i.e., the case where the localized monomer is at the midpoint along the contour of the polymer. At each value of $m_{\rm loc}$, the free energy increases with increasing cavity size.

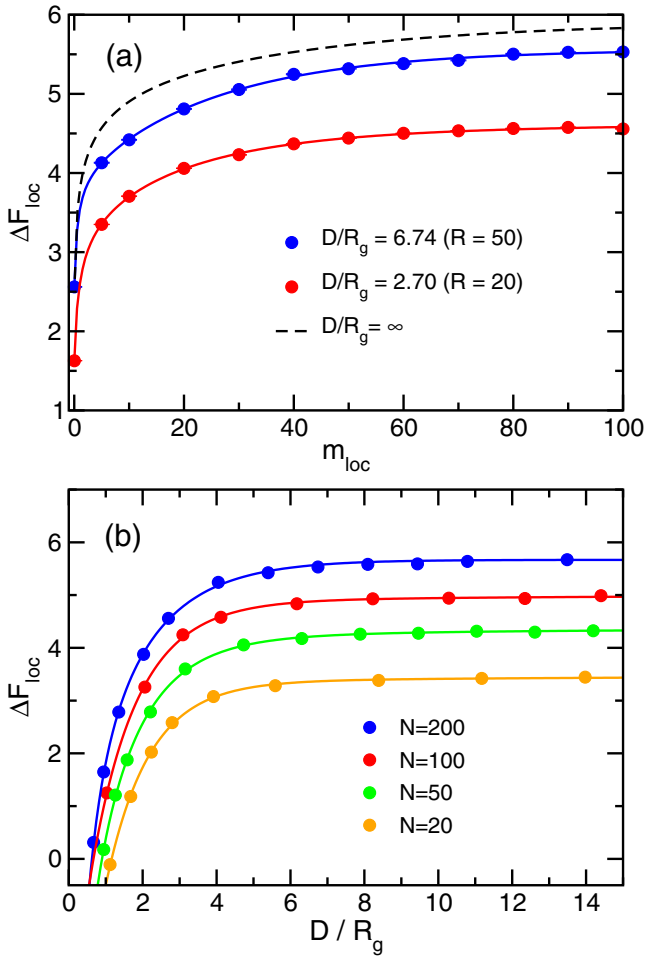

FIG. 7. (a) $\Delta F_{\rm loc}$ vs scaled confining cavity size $D/R_{\rm g}$, where $\Delta F_{\rm loc}$ is the free-energy cost of localizing a middle monomer to a point in the center of a face on a confining cubic surface. Results are shown for polymer chains of length $N = 20$, 50, 100, and 200. The dashed line shows the theoretical prediction of Eq. (26) for the limiting case of $D/R_{\rm g} \to \infty$. The constant in Eq. (26) is chosen simply to shift the theoretical curve above the simulation data for clarity. (b) $\Delta F_{\rm loc}$ vs monomer localization index $m_{\rm loc}$ for a $N = 200$ polymer confined to a spherical cavity. Results for different spherical cavity sizes are shown.

Figure 7(b) shows the variation of $\Delta F_{\rm loc}$ with cavity size in the case of localization of the central monomer, i.e., $m_{\rm loc} = N/2$. Results are shown for different polymer lengths. The general trends are qualitatively consistent with the results in Fig. 3 for end-monomer localization; that is, $\Delta F_{\rm loc}$ increases rapidly with D for $D/R_{\rm g} \lesssim 3$ and gradually levels off for larger D, and it increases with increasing N. The origins of these effects are the same as those discussed for end-monomer localization.

Figure 8 shows the variation of the free energy with chain length in the case of $m_{\rm loc} = N/2$ for a polymer confined to a spherical cavity. Results are shown for cavity sizes of $D/R_{\rm g} = 2.5$ and 10. For a helpful comparison, the free energy for a polymer with end-monomer localization ($m_{\rm loc} = 0$) is also shown. We find that $\Delta F_{\rm loc}$ varies linearly with $\ln N$, as was the case in Fig. 4 for end-monomer localization inside a cube. The solid curves in the figure are fits to the function

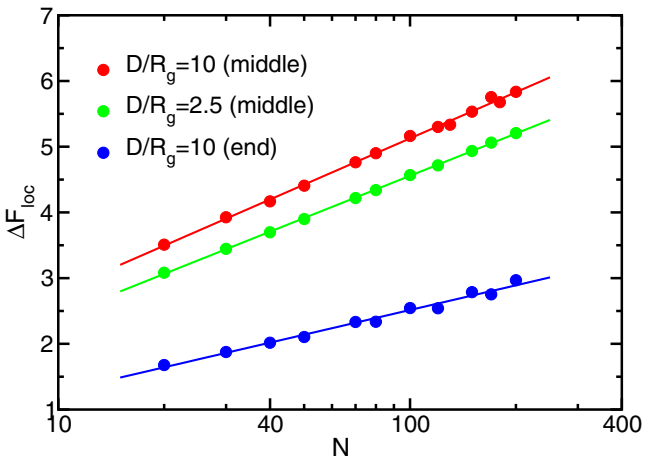

FIG. 8. $\Delta F_{\rm loc}$ vs polymer length N for a polymer confined to a sphere in the case of localization of the middle monomer of the polymer. Results are shown for $D/R_{\rm g} = 2.5$ and 10. For convenient comparison, results are also shown for end-monomer localization with $D/R_{\rm g} = 10$. The curves overlaid on the data are fits to $\Delta F_{\rm loc} = c + \alpha \ln N$. The fitting parameter values are as follows for localization of the middle monomer: $\alpha = 1.01 \pm 0.02$ and $c = 0.46 \pm 0.07$ for $D/R_{\rm g} = 10$ and $\alpha = 0.928 \pm 0.005$ and $c = 0.28 \pm 0.02$ for $D/R_{\rm g} = 2.5$. For end-monomer localization with $D/R_{\rm g} = 10$, $\alpha = 0.54 \pm 0.02$ and $c = 0.0 \pm 0.1$.

$\Delta F_{\rm loc} = c + \alpha \ln N$. For $m_{\rm loc} = N/2$, we find that $\alpha = 1.01 \pm 0.02$ for $D/R_{\rm g} = 10$ and $\alpha = 0.928 \pm 0.05$ for $D/R_{\rm g} = 2.5$. By contrast, we find that $\alpha = 0.54 \pm 0.02$ for $m_{\rm loc} = 0$ and $D/R_{\rm g} = 10$.

An explanation for the variation in $\Delta F_{\rm loc}$ with localization position is given as follows. Consider first the case of a very large confining cavity, in which case the confining surface near the localization point is effectively flat. Next, note that a polymer with monomer $m_{\rm loc}$ localized to a point on the wall corresponds to two subchains of length $m_{\rm loc}$ and $N - m_{\rm loc}$, each connected to this point. As noted earlier, the partition function for a single self-avoiding chain tethered to a point on an infinite flat wall is $Z_1(N) = q^N N^{\gamma_1 - 1}$, where $\gamma_1 \approx 0.69$ and where q is the effective coordination number of the random walk. Thus, in the hypothetical case where the two subchains interact internally but not with each other, the partition function is $Z(m_{\rm loc}) = Z_1(m_{\rm loc}) Z_1(N - m_{\rm loc})$ or

$$Z(m_{\rm loc}) = q^N (m_{\rm loc}(N - m_{\rm loc}))^{\gamma_1 - 1}. \tag{24}$$

For localization at the midpoint of $m_{\rm loc} = N/2$, this becomes $Z(m_{\rm loc}) = q^N (N/2)^{2\gamma_1 - 1}$. As noted in Ref. [23], interactions between the subchains leads to a modified scaling of $Z \sim q^N (N/2)^{\gamma_2 - 1}$, where $\gamma_2 \approx 0.203$. Thus, for $m_{\rm loc} = N/2$, we find that $F/k_{\rm B}T = -\ln Z = (1 - \gamma_2) \ln(N) - N \ln q + \text{const}$. Since the partition function of a free self-avoiding polymer scales as $Z_0 \sim q^N N^{\gamma_0 - 1}$, where $\gamma_0 \approx 1.16$, it follows that the difference in the conformational free energy for a free polymer and one with the middle monomer localized to a point on a flat surface is given by

$$\Delta F/k_{\rm B}T = (\gamma_2 - \gamma_1) \ln N + \text{const.}, \tag{25}$$

where $\gamma_2 - \gamma_0 = 0.96$. This scaling is expected for the free-energy cost of localizing a middle monomer in the limit of infinitely large confinement cavity and for a sufficiently long chain. This scaling factor is close to the value of $\alpha = 1.01 \pm 0.02$ observed for the large cavity size of $D/R_g = 10$. As noted earlier, in the case of end-monomer localization, the corresponding prediction for the localization free energy is $\Delta F = 0.47 \ln N$. This is comparable to the observed scaling of $\Delta F_{loc} = (0.54 \pm 0.02) \ln N$ + constant observed for end-monomer localization in a spherical cavity of size $D/R_g = 10$. As before, the small differences between the predicted and observed scaling are attributable to finite-size effects associated with the finite cavity size and the polymer length.

To account for the variation of ΔF_{loc} with m_{loc} observed in Fig. 7(a), we follow Ref. [22] and note that application of Duplantier's theory of polymer networks [24] leads to a modification of Eq. (24) to $Z(m_{loc}) \sim q^N m_{loc}^{\gamma_2-\gamma_1} (N - m_{loc})^{\gamma_1-1}$. Consequently, the localization free energy, $\Delta F_{loc}(m_{loc})/k_B T = -\ln(Z/Z_0)$, can be written as

$$\Delta F_{loc}/k_B T = 0.49 \ln m_{loc} + 0.31 \ln(N - m_{loc}) + c(N), \tag{26}$$

where $c(N) = 0.16 \ln N + c_0$ and where c_0 is an unknown constant. The theoretical prediction for $\Delta F_{loc}(m_{loc})$ is plotted in Fig. 7 using a constant of $c_0 = 1.3$ to shift the curve above the simulation data for clarity. The predicted function is comparable to the measured $\Delta F_{loc}(m_{loc})$.

C. End-monomer localization of a tethered polymer

Let us now consider the case of localization of an end monomer for confinement inside a sphere in the case where the other end monomer is already tethered to a point on the surface. Figure 9 shows ΔF_{loc} vs cavity size D for a polymer of length $N = 200$. Results are shown for both real and ideal polymers and for four values of the angle θ between the tethering point and the localization point on the sphere. Several trends are evident. As expected, the free energy increases monotonically with increasing sphere size, due mainly to the stretching of the polymer. In addition, at fixed D the free energy increases with increasing θ. This results from the increase in the distance between tethering points with θ, leading to further stretching of the polymer. The effect of including monomer-monomer repulsion leads to a decrease in the free energy relative to the case for ideal polymers. This arises because such repulsions lead to a swelling of the chain, leading to a tendency for the free end monomer to lie on average further away from the tethered end monomer and thus closer to the point where the free monomer is localized. Concomitantly, the probability that it lies at that point is greater and thus the localization free energy is lower.

Another noteworthy feature of the data in Fig. 9 is the fact that localization free energy levels off for real chains in the range $D \lesssim 30$ and appears to approach a minimum for ideal chains at $D \approx 10$. The significance of this trend can be understood by noting that the effective diameter of the unconfined polymer is $2R_g = 23.9$ for a real polymer and $2R_g = 12.4$ for an ideal polymer. In each case, it is expected that the free-energy cost of pulling the ends of a polymer a distance $\lesssim 2R_g$ will be roughly independent distance and of

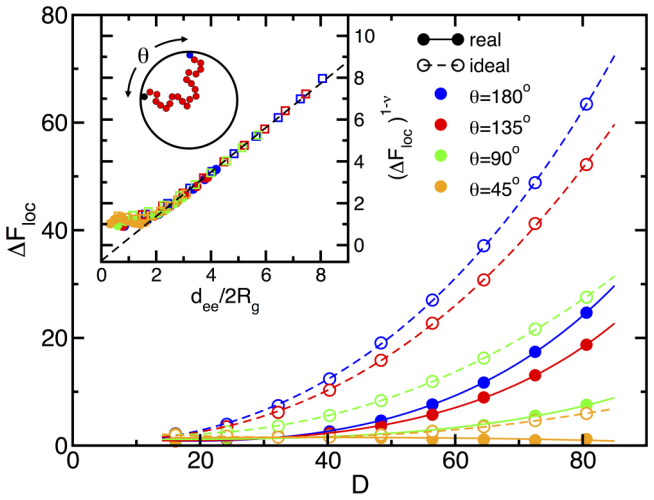

FIG. 9. ΔF_{loc} vs confining sphere diameter D for a chain of length $N = 200$. Here, ΔF_{loc} is the change in the conformational free energy upon localizing a monomer to a point on the inner surface of the sphere in the case where the other monomer is tethered to a different point on the sphere. Results are shown for four different values of the angular distance θ between the tethered point and the localization point for real (i.e., self-avoiding) polymers and ideal polymers (for which the excluded-volume interaction between nonbonded monomers is turned off). The inset shows the scaled free energy $(\Delta F_{loc})^{1/(1-\nu)}$ vs scaled end-to-end distance $d_{ee}/2R_g$ where $d_{ee} \equiv (6/\pi)^{1/3} D \sin(\theta/2)$. The results were calculated using the raw data with $\nu = \frac{1}{2}$ for ideal chains and $\nu = \frac{3}{5}$ for real chains. The dashed curve is a linear fit to the data in the domain $d_{ee}/2R_g > 1.7$. The illustration in the inset shows the definition of the angle θ.

the order of $k_B T$ and independent of distance. Only when the distance exceeds this value will the polymer become appreciably distorted in shape. Consequently, the free energy is expected to rise considerably only after that point.

In order to carry out a quantitative analysis of the data, we employ a standard expression for the scaling of the free energy of a stretched polymer of length N with distance d_{ee} between the ends of the polymer [25]: $\Delta F/k_B T \sim (d_{ee}/R_g)^{1/(1-\nu)}$. Note that this relation employs the de Gennes blob picture and is only expected to be valid when d_{ee} exceeds the average size of the free polymer, for which we choose $2R_g$ as a convenient measure. Consequently, $(\Delta F/k_B T)^{1-\nu}$ will scale linearly with d_{ee} only for $d \gtrsim 2R_g$. In applying this result to the present analysis, we initially assume that confinement effects are weak and also note that the distance d_{ee} scales with θ as $d_{ee} = (6/\pi)^{1/3} D \sin(\theta/2)$, where the factor of $(6/\pi)^{1/3}$ arises from the definition of $D \equiv V^{1/3}$. This leads to the prediction that $(\Delta F_{loc})^{1-\nu}$ varies linearly with $d_{ee}/2R_g$ and, further, that the data collapses to a single curve for all values of θ and for real and ideal polymers. The inset of Fig. 9 shows that this prediction is borne out since the data collapse to a single linear curve for $d_{ee}/2R_g \gtrsim 1.7$. This result is somewhat surprising for two reasons. First, it suggests that the confinement effects omitted from this analysis are not significant relative to the effects of stretching the polymer, at least in the regime where the end-to-end distance exceeds the mean size of the free polymer. In addition, for the larger values of θ and sphere size D, the end-to-end stretch distance

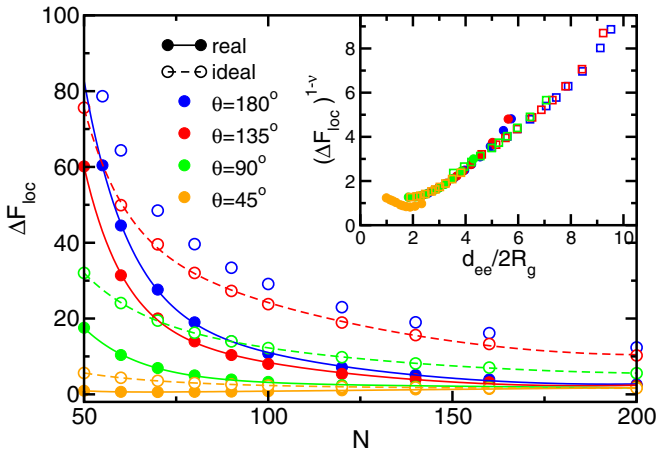

FIG. 10. As in Fig. 9, except $\Delta F_{\rm loc}$ vs polymer length N for confinement in a sphere of diameter $D = 50$. The inset shows $(\Delta F_{\rm loc})^{1-\nu}$ vs $d_{\rm ee}/2R_{\rm g}$, calculated as for the data in the inset of Fig. 9.

is an appreciable fraction of the contour length. This leads to small blob sizes and eventually a breakdown in the whole blob picture that underlies the scaling relation we employ.

Figure 10 shows the variation of $\Delta F_{\rm loc}$ with polymer length N for a fixed sphere diameter of $D = 50$. We consider chain lengths in the range of $N = 50$–200. As in Fig. 9, results are shown for various values of θ and for both real and ideal chains. As expected, the localization free-energy cost increases as the chain length decreases and, thus, as the relative degree of deformation of the polymer from its undistorted shape increases. Consistent with the previous results and for the same reasons outlined above, $\Delta F_{\rm loc}$ increases with increasing θ and is lower for real chains than for ideal chains. The inset shows $(\Delta F_{\rm loc})^{1-\nu}$ vs $d_{\rm ee}/2R_{\rm g}$. By comparison with Fig. 9, we note that the scaling of the data yields poorer collapse of the data and a less linear variation of $(\Delta F_{\rm loc})^{1-\nu}$ with the end-to-end distance. The deviations from such trends are especially evident for the data points corresponding to large $d_{\rm ee}$, which here corresponds to the shortest chain lengths. We believe that this is mainly due to a finite-size effect due to small N and propose that better data collapse and more linear functions would emerge using polymer lengths much greater than we can feasibly examine at present.

VI. CONCLUSIONS

In this study, we have presented and tested a Monte Carlo simulation method for calculating the free energy cost of localizing a single monomer of a confined polymer to a point on the inner surface of the confining cavity. The core element of this method involves measuring the probability that the chosen monomer lies in a volume $V_{\rm b}$, which is a subvolume of a larger volume $V_{\rm a}$ within which the monomer is confined in a given simulation. The volume $V_{\rm a}$ is itself a subvolume of the cavity volume V. By carrying out a sequence of simulations in which $V_{\rm a}$ is varied from V to a very small volume situated at the localization point, summing the resulting free energy differences, and subtracting out the translational free energy of the monomer, the localization free energy $\Delta F_{\rm loc}$ is calculated.

Using this approach, we measured $\Delta F_{\rm loc}$ for localization of an end monomer to sites on spherical and square confining surfaces and, in the latter case, to sites at the center of a cube face and at a cube corner. For a strongly confined polymer with $D \lesssim 2R_{\rm g}$, $\Delta F_{\rm loc}$ is negligible. As the confinement size D increases, $\Delta F_{\rm loc}$ initially increases rapidly and then levels off asymptotically in the weak confinement limit of $D \gg R_{\rm g}$. The free-energy cost is significantly higher for end-monomer localization to the corner of a cube than for localization to a cube face center, as expected from the greater deformation of polymer chain that results for the former case. In all cases, $\Delta F_{\rm loc}$ increases monotonically with chain length N and generally scales as $\Delta F_{\rm loc} = m \ln N +$ constant. At sufficiently large $D/R_{\rm g}$, the proportionality constant m is consistent with the prediction that uses the known form of the partition function of a self-avoiding chain in a scalefree environment, $Z \sim q^N N^{1-\gamma}$, along with the known or measured values of the exponent γ for a free polymer and a polymer end tethered to a flat wall or corner. In addition, a simple theoretical model yielded scaling results of $\Delta F_{\rm loc}$ with respect to N and D that are semiquantitatively consistent with the simulation results. Specifically, we find the following qualitative consistencies: a rapid decrease in $\Delta F_{\rm loc}$ as the cavity size decreases for $D/R_{\rm g} \lesssim 4$, a greater value of $\Delta F_{\rm loc}$ for tethering to a cube corner compared to that for a cube face, and a value higher of $\Delta F_{\rm loc}$ for localization to a sphere compared to the face of a cube of the same volume. In addition, we find the scaling factor characterizing the linear variation of $\Delta F_{\rm loc}$ with N to be quantitatively close to the predicted value. The small discrepancy between the calculated and predicted variation of $\Delta F_{\rm loc}$ with D and N for arbitrary $D/R_{\rm g}$, which is typically $<1\ k_{\rm B}T$, arises from the simplicity of the theoretical model employed.

We also examined the case of localization of a monomer at arbitrary position along the polymer contour and obtained results that are qualitatively similar to those for end-monomer localization and quantitatively consistent with theoretical predictions. This consistency provides a clear demonstration of the validity and accuracy of the method. Finally, we examined end-monomer localization in the case where the other polymer end is tethered to a different point on the confinement surface. We find that the variation of $\Delta F_{\rm loc}$ with D for a sufficiently long polymer is consistent with the standard theoretical predictions for an unconfined stretched polymer using the blob model. This suggests that the effect of confinement in this case is not significant, at least for tethering point distances that exceed the average polymer size of $\sim 2R_{\rm g}$.

All calculations in this work used a freely jointed hard-sphere chain confined to a spherical or cubic cavity. Employing such a simple model was useful for demonstrating the validity and utility of the method and for facilitating easy comparison with theoretical predictions. In future work, it will be of interest to examine more complex models and consider the effects of features such as polymer bending rigidity, macromolecular crowding, and polymer topology (e.g., ring or branched). It will also be useful to examine monomer localization for polymers confined to cavities of a variety of types, including anisometrically shaped cavities [5] and pyramidal cavities [16]. Finally, these calculations can be used to test directly those theories of polymer translocation that

emphasize the importance of the free-energy barrier on the translocation dynamics as the localization free energy can be calculated for any model used in dynamics simulations.

ACKNOWLEDGMENTS

This work was supported by the Natural Sciences and Engineering Research Council of Canada (NSERC). We are grateful to Compute Canada and the Atlantic Computational Excellence Network (ACEnet) for use of their computational resources.

APPENDIX A: FREE ENERGY OF FREE AND TETHERED POLYMERS

In this Appendix, we calculate the conformational free energies for (a) a free polymer, F_a, (b) a polymer tethered to an infinitely wide flat hard wall, F_b, and (c) a polymer tethered to a corner of an infinitely large hard-walled cube, F_c. These are used to obtain the free-energy differences $\Delta F_{ab} \equiv F_b - F_a$, $\Delta F_{ac} \equiv F_c - F_a$, and $\Delta F_{bc} = F_c - F_b$, which are used in the model developed in Appendix C to estimate the chain-end localization free energy for a polymer under confinement in a cavity of arbitrary size. In the limit of large N, it is known that the partition function for such scalefree polymer systems has the form $Z_i = q^N N^{\gamma_i - 1}$, where the effective coordination number q is related to the chemical potential per monomer μ by $q = e^{-\beta\mu}$. In addition, the scaling exponent γ_i depends on the constraints, if any, imposed on the polymer. For a free polymer (i = a), $\gamma_a = 1.16$, while for a polymer tethered to wall (i = b), $\gamma_b = 0.69$. Noting that $\beta F_i = -\ln Z_i$, it follows that the free-energy difference $\Delta F_{ab} = F_b - F_a$ is $\Delta F_{ab} = (\gamma_a - \gamma_b)\ln N = 0.47 \ln N$. Since the functional form of F_i and the values of γ_a and γ_b are strictly correct only in the limit of very large N, the use of short polymer lengths here (N = 20–200) is expected to lead to finite-size effects that may alter the form for F_i and/or the effective scaling exponents. In addition, to our knowledge the value of γ_c has not been measured. For these reasons, it is of interest to calculate F_a, F_b, and F_c directly for the range of N relevant to this study.

We employ the pruned-enriched-Rosenbluth method (PERM) to directly calculate F_a, F_b and F_c, which then yield all three free energy differences. The PERM simulations are implemented in the same manner described in Ref. [26]. Figure 11 shows the variation of ΔF_{ab}, ΔF_{ac}, and ΔF_{bc} with polymer length. The inset shows F_a, F_b, and F_c used to calculate the differences. The dotted curves in the main figure overlaid on the data are fits to the function $\Delta F_{\lambda\mu} = C_{\lambda\mu} + \alpha_{\lambda\mu} \ln N$ in the range N = 10–200. We find that the best-fit parameter values of $C_{ac} = 1.476 \pm 0.004$, $\alpha_{ac} = 1.451 \pm 0.001$; $C_{bc} = 1.031 \pm 0.002$, $\alpha_{bc} = 1.006 \pm 0.001$; and $C_{ab} = 0.444 \pm 0.002$, $\alpha_{ab} = 0.446 \pm 0.002$. The values for ΔF_{ab} compare well with the values obtained using the SCH method in Fig. 12.

Checking the validity of the expressions for α_{ac} and α_{bc} requires a value for γ_c, the exponent for a corner-tethered polymer. We are unaware of any calculation of this exponent. However, we do note that in Refs. [27] and [28] the quantity $\alpha_{bc'} \equiv \gamma_{c'} - \gamma_b$ was calculated using lattice Monte Carlo simulations for self-avoiding walk, where $\gamma_{c'}$ is the exponent for a polymer whose end is tethered to a tip of a hard conical

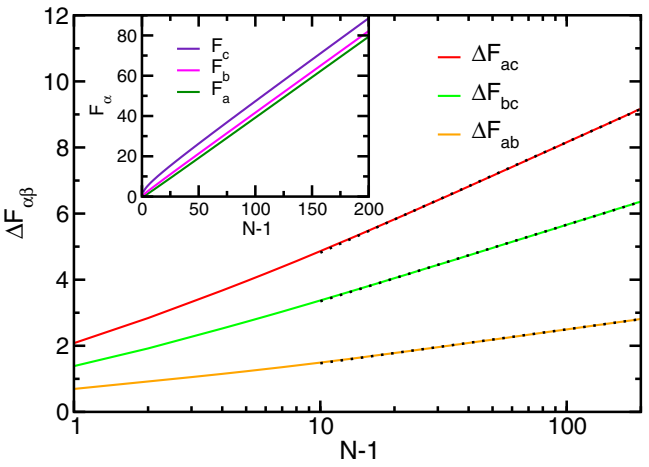

FIG. 11. Free-energy differences vs polymer length calculated from PERM simulations. These differences are defined $\Delta F_{ab} \equiv F_b - F_a$, $\Delta F_{ac} \equiv F_c - F_a$, and $\Delta F_{bc} \equiv F_c - F_b$, where (i) F_a is the free energy of a free polymer; (ii) F_b is that for a polymer tethered to a hard flat wall, and (iii) F_c is that for a polymer tethered to a corner of an infinitely large confining cube. The dashed lines overlaid on the curves are fits to the function $\Delta F_{\lambda\mu} = C_{\lambda\mu} + \alpha_{\lambda\mu} \ln N$, where $C_{ac} = 1.476 \pm 0.004$, $\alpha_{ac} = 1.451 \pm 0.001$; $C_{bc} = 1.031 \pm 0.002$, $\alpha_{bc} = 1.006 \pm 0.001$; and $C_{ab} = 0.444 \pm 0.002$, $\alpha_{ab} = 0.446 \pm 0.002$. The inset shows the free energies F_a, F_b, and F_c vs N.

object. Choosing a cone half-angle $\Theta = 0.77\pi > \pi/2$ means that the tethered polymer confined to lie in a conical subspace with a half-angle of 0.23π, which has a solid angle equal to that of the corner-tethered system of $\Omega = \frac{1}{8}(4\pi)$. From Fig. 3 of Ref. [27] the exponent difference is estimated to be $\alpha_{ac} \equiv \gamma_c - \gamma_a \approx 1.4$. This is close to the value of 1.451 obtained from the PERM simulations for a corner-tethered polymer.

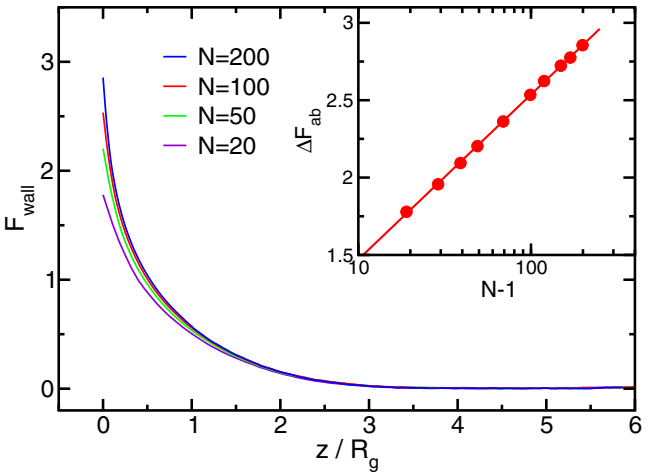

FIG. 12. Conformational free energy of a polymer near a flat wall F_{wall} vs scaled distance of an end monomer away from the wall, z/R_g. Results are shown for different polymer lengths. The inset shows the difference $\Delta F_{ab} \equiv F_{wall}(0) - F_{wall}(\infty)$ vs N. The solid line shows the fit to $\Delta F_{ab} = C_{ab} + \alpha_{ab} \ln N$, which yields $\alpha_{ab} = 0.463 \pm 0.003$ and $C_{ab} = 0.40 \pm 0.01$.

APPENDIX B: FREE ENERGY VERSUS END-MONOMER POSITION FROM A FLAT WALL

In this Appendix, we calculate the variation of the conformational free energy with the distance z of the end monomer from an infinitely wide hard flat wall. We employ the self-consistent histogram (SCH) method [29], which we have previously used to calculate free-energy functions for other processes such as polymer translocation [19]. Figure 12 shows the variation of the free energy of a polymer as a function of the distance of one end monomer away from the wall. Results are shown for polymers of length $N = 20$, 50, 100, and 200, and the distance is scaled with respect to R_g, the radius of gyration of a free polymer. As expected, the free energy rises monotonically as the polymer approaches the wall as a result of a decrease in conformational entropy. In addition, the free energy levels off to a constant value at distances far from the wall. Upon approaching the wall, the distance at which the free energy becomes appreciable relative to k_BT is $z \approx R_g$. We note that near the wall the free energy increases slightly with increasing polymer length. Note that the quantity $\Delta F_{ab} \equiv F_{wall}(0) - F_{wall}(\infty)$ is the free-energy difference between a free and a wall-tethered polymer. The inset of the figure shows ΔF_{ab} vs N for the range $N = 20$–200. The solid line is a fit to the function $\Delta F_{ab} = C_{ab} + \alpha_{ab} \ln N$, which yielded best-fit parameter values of $\alpha_{ab} = 0.463 \pm 0.003$ and $C_{ab} = 0.40 \pm 0.01$. The value for α_{ab} compares well with the predicted value of 0.47 and the value of the 0.446 ± 0.002 measured using PERM simulations in Appendix A.

APPENDIX C: DERIVATION OF EQUATIONS FOR THE THEORETICAL MODEL

In this Appendix, we develop the theoretical model used to understand the scaling of the localization free energy with N and confining cavity size, as well as the cavity shape and location of the localization point on the cavity surface. We first develop an approximation for the free-energy cost of localizing an end monomer to a point on the wall of the confining cube located at the center of one of the cube faces. In practice, the validity of the derived result does not require that it be exactly at the center but rather only that it not be too close to one of the corners of the cube.

Consider a cubic box of dimension D and volume $V = D^3$ within which a polymer is confined. The probability distribution for the position of an end monomer $\mathbf{R}_0$ is

$$P(\mathbf{R}_0) = \frac{e^{-\beta F(\mathbf{R}_0)}}{\int_V d^3\mathbf{R}_0 e^{-\beta F(\mathbf{R}_0)}}, \tag{C1}$$

where $F(\mathbf{R}_0)$ is the conformational free energy of the polymer for this end-monomer position. If the confining cube is sufficiently large relative to the average polymer size, then there exists an interior region of the cube where a polymer located inside does not appreciably interact with the walls of the box. Let us call this region A and its volume $V_a(<V)$. If the end monomer lies within this subspace, we expect the conformational free energy of the polymer to be otherwise independent of position. Call this free energy F_a. Outside this subspace is a layer of width $\Delta D \approx R_g$ adjacent to the walls of the box. Let us write $\Delta D = \mu R_g$, where the dimensionless

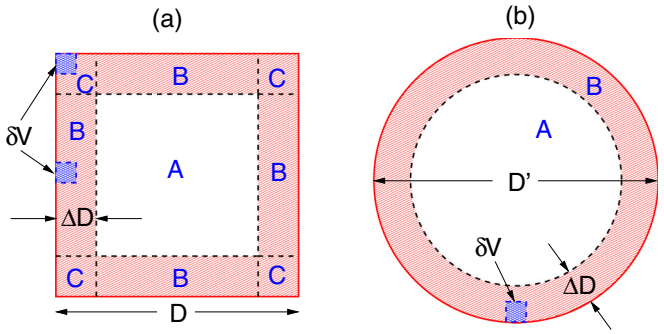

FIG. 13. Illustration of the various quantities used for the theoretical model. (a) Region A is cubic subspace of the confining cube. Region C is composed of eight small cubes near the corners of the confining cube, and region B is the remaining subspace located near the walls of the cube. When a polymer is located in region A, it does not interact with the walls of the box. However, when it is located in regions B or C, it does interact, leading to an increase in the conformational entropy, as explained in the text. (b) As in panel (a), except for a confining sphere. There is only a single region (B) where the polymer interacts with the confining wall. Note that $D' = (4\pi/3)^{1/3} D$, as explained in the text.

scaling factor μ is of order unity. We divide this region into two smaller regions. Region C is comprised of the eight cubes, each of side length μR_g, that lie in the corners of the confining cube. Region B is composed of the six regions near the wall that lie further away from the corners of the cube. If the end monomer lies at a position inside regions B and C, the polymer interacts with the walls of the box and the reduction of the conformational entropy causes the free energy to be greater than F_a. The free-energy will, of course, depend on the exact location of the end monomer inside this layer, i.e., how close it is to the wall or corner. For simplicity, we model this effect by choosing a free energy that is taken to be constant in each subspace, which we label F_b and F_c for regions B and C, respectively. Figure 13(a) illustrates the regions of the confining cube.

Consider the case where the end monomer lies in region B. From Eq. (C1), it follows that the probability distribution for $\mathbf{R}_0$ is then

$$P_b(\mathbf{R}_0) = \frac{e^{-\beta F_b}}{V_a e^{-\beta F_a} + V_b e^{-\beta F_b} + V_c e^{-\beta F_c}} \quad (\mathbf{R}_0 \text{ in B}). \tag{C2}$$

The probability that the end monomer lies in a smaller subspace of region B of volume δV is determined by integration: $P(\delta V) = \int_{\delta V} d^3\mathbf{R}_0 P(\mathbf{R}_0)$. It can be shown that this leads to

$$P_b(\delta V) = \frac{(\delta V/V)}{(V_a/V)e^{\beta \Delta F_{ab}} + (V_b/V) + (V_c/V)e^{\beta \Delta F_{cb}}}, \tag{C3}$$

where $\Delta F_{ab} \equiv F_b - F_a$ and $\Delta F_{cb} \equiv F_b - F_c$.

The total free energy cost of confinement of the end monomer to δV is $F_{conf} = -\ln P_b(\delta V)$. Consequently,

$$F_{conf} = \ln(V/\delta V) + \Delta F_{loc}, \tag{C4}$$

where the first term is equivalent to the free energy cost of localizing a hypothetical detached end monomer. The second

term, defined

$$\Delta F_{\rm loc}/k_{\rm B}T \equiv \ln[(V_{\rm a}/V)e^{\beta\Delta F_{\rm ab}} + (V_{\rm b}/V) + (V_{\rm a}/V)e^{\beta\Delta F_{\rm cb}}], \tag{C5}$$

accounts for the attachment of the end monomer to the rest of the polymer, whose conformational entropy is determined by the end-monomer location. This, of course, is the approximation for the chain-end localization free energy. Note that in the limit of very large confinement volume the boundary layer regions B and C become negligible by comparison, i.e., $V_{\rm a}/V \to 1$, $V_{\rm b}/V \to 0$, and $V_{\rm c}/V \to 0$, and thus $\Delta F_{\rm loc} = \Delta F_{\rm ab}$, as expected.

Next, we make the following approximations for $\Delta F_{\rm ab}$ and $\Delta F_{\rm cb}$ $(= -\Delta F_{\rm bc})$. First note that the quantities $F_{\rm a}$, $F_{\rm b}$ and $F_{\rm c}$ are the conformational free energies of the polymer (assumed constant) for end-monomer position in each or the three regions. Approximating each of these as the free energies of a free polymer ($F_{\rm a}$) or an end-tethered polymer to a large flat wall or corner ($F_{\rm a}$ and $F_{\rm c}$, respectively), we write

$$\Delta F_{\lambda\mu}/k_{\rm B}T = C_{\lambda\mu} + \alpha_{\lambda\mu}\ln N \tag{C6}$$

and use the values of $C_{\rm ab}$, $C_{\rm cb}$, $\alpha_{\rm ab}$, and $\alpha_{\rm cb}$ obtained from the PERM simulations in Appendix A. Note that the use of the scaling results from Appendix A is strictly correct only for very large confinement cubes ($R_{\rm g} \ll D$) and for end-monomer locations that lie on the confining surface, rather than at arbitrary position in regions B and C, as assumed here.

Finally, let us define the ratio $r \equiv D/R_{\rm g}$, where $R_{\rm g}$ is the radius of gyration. Since the subspaces B and C constitute a layer of width $\Delta D = \mu R_{\rm g}$ near the walls of the cube, the volume $V_{\rm a}$ is given by $V_{\rm a} = (D - 2\mu R_{\rm g})^3$. In addition, $V_{\rm c} = 6(\mu R_{\rm g})^3$ and $V_{\rm b} = V - V_{\rm a} - V_{\rm b}$. It follows that

$$\begin{aligned} V_{\rm a}/V &= 1 - 6\mu r^{-1} + 12\mu^2 r^{-2} - 8\mu^3 r^{-3}, \\ V_{\rm b}/V &= 6\mu r^{-1} - 12\mu^2 r^{-2}, \\ V_{\rm c}/V &= 8\mu^3 r^{-3}. \end{aligned} \tag{C7}$$

The conformational free-energy cost of localizing an end monomer to a point near a wall, $\Delta F_{\rm loc}$ is approximated using Eqs. (C5)–(C7). We use these equations to estimate the free energy of localization to a point in the middle of one of the cube faces. For the calculations used to generate the results in Figs. 5 and 6, we use a value for the dimensionless factor μ appearing in Eqs. (C7) of $\mu = 0.7$. The results of Fig. 12 in Appendix B demonstrate that this is a reasonable choice. Using other values of order unity has a small quantitative effect on the predictions, but the qualitative trends are unaltered.

Next, we consider end-monomer localization near a corner of the box. If the end monomer lies in region C, the probability distribution for $\mathbf{R}_0$ is

$$P(\mathbf{R}_0) = \frac{e^{-\beta F_{\rm c}}}{V_{\rm a}e^{-\beta F_{\rm a}} + V_{\rm b}e^{-\beta F_{\rm b}} + V_{\rm c}e^{-\beta F_{\rm c}}}. \tag{C8}$$

The probability that $\mathbf{R}_0$ lies in a small volume δV located in region C is obtained from integration, $P_{\rm c}(\delta V) = \int_{\delta V} P(\mathbf{R}_0)d^3\mathbf{R}_0$. It can then be shown that the total free-energy cost of end-monomer confinement to δV is $F_{\rm conf} = -\ln P_{\rm c}(\delta V) = \ln(V/\delta V) + \Delta F_{\rm loc}$, where the end-monomer localization free energy is given by

$$\Delta F_{\rm loc}/k_{\rm B}T = \ln[(V_{\rm a}/V)e^{\beta\Delta F_{\rm ac}} + (V_{\rm b}/V)e^{\beta\Delta F_{\rm bc}} + (V_{\rm c}/V)], \tag{C9}$$

where $\Delta F_{\rm ac} \equiv F_{\rm c} - F_{\rm a}$ and $\Delta F_{\rm bc} \equiv F_{\rm c} - F_{\rm b}$. These free-energy differences are approximated once again using Eq. (C6), where the quantities $C_{\lambda\mu}$ and $\alpha_{\lambda\mu}$ are obtained from the fits to the PERM simulation data of Appendix A.

The free-energy cost for end-monomer localization to a corner of the cube is approximated using Eqs. (C6), (C7), and (C9). As noted above, to generate the results in Figs. 5 and 6 we use a value for the scaling factor of $\mu = 0.7$.

Finally, let us consider the case of end-monomer localization of a point on the wall of a confining sphere. Unlike the case of the cube, we need only define a single region for which the polymer interacts with the confining wall. We denote the interior region A and the outer region B, as illustrated in Fig. 13(b). Following the same approach as above, it is easy to show that the localization free energy is given by

$$\Delta F_{\rm loc}/k_{\rm B}T \equiv \ln[(V_{\rm a}/V)e^{\beta\Delta F_{\rm ab}} + (V_{\rm b}/V)], \tag{C10}$$

where

$$\begin{aligned} V_{\rm a}/V &= 1 - 6\mu(c/r) + 12\mu^2(c/r)^2 - 8\mu^3(c/r)^3, \\ V_{\rm b}/V &= 6\mu(c/r) - 12\mu^2(c/r)^2 + 8\mu^3(c/r)^3, \end{aligned} \tag{C11}$$

and where $c \equiv (\pi/6)^{1/3}$. Note that since $D \equiv V^{1/3}$, it follows that the confining sphere diameter D' is given by $D' = (\pi/6)^{1/3}D$, which is the origin of the factor c in these equations. As before, $F_{\rm ab}$ is determined by Eq. (C6), and we use $\mu = 0.7$.

[1] M. Muthukumar and A. Baumgärtner, Macromolecules **22**, 1937 (1989).

[2] M. Muthukumar, Phys. Rev. Lett. **86**, 3188 (2001).

[3] M. Muthukumar, J. Chem. Phys. **118**, 5174 (2003).

[4] C. Y. Kong and M. Muthukumar, J. Chem. Phys. **120**, 3460 (2004).

[5] J. M. Polson, J. Chem. Phys. **142**, 174903 (2015).

[6] M. Magill, E. Waller, and H. W. de Haan, J. Chem. Phys. **149**, 174903 (2018).

[7] N. Laachi and K. D. Dorfman, J. Chem. Phys. **132**, 084108 (2010).

[8] C. J. Rasmussen, A. Vishnyakov, and A. V. Neimark, J. Chem. Phys. **137**, 144903 (2012).

[9] E. J. Saltzman and M. Muthukumar, J. Chem. Phys. **131**, 214903 (2009).

[10] Z. E. Dell and M. Muthukumar, J. Chem. Phys. **149**, 174902 (2018).

[11] B. Alberts, A. Johnson, J. Lewis, M. Raff, K. Roberts, and P. Walters, *Molecular Biology of the Cell*, 5th ed. (Garland Science, New York, 2008).

[12] H. Lodish, A. Berk, C. A. Kaiser, M. Krieger, A. Bretscher, H. Ploegh, A. Amon, and M. P. Scott, *Molecular Cell Biology*, 7th ed. (W. H. Freeman and Company, New York, 2012).

[13] D. Nykypanchuk, H. H. Strey, and D. A. Hoagland, Science **297**, 987 (2002).

[14] N. Laachi and K. D. Dorfman, J. Chem. Phys. **133**, 234104 (2010).
[15] M. Magill, C. Falconer, E. Waller, and H. W. de Haan, Phys. Rev. Lett. **117**, 247802 (2016).
[16] M. Langecker, D. Pedone, F. C. Simmel, and U. Rant, Nano Lett. **11**, 5002 (2011).
[17] M. Muthukumar, *Polymer Translocation* (CRC Press, Boca Raton, FL, 2011).
[18] W. Sung and P. J. Park, Phys. Rev. Lett. **77**, 783 (1996).
[19] J. M. Polson, M. F. Hassanabad, and A. McCaffrey, J. Chem. Phys. **138**, 024906 (2013).
[20] C. J. Rasmussen, A. Vishnyakov, and A. V. Neimark, J. Chem. Phys. **135**, 214109 (2011).
[21] A. Cacciuto and E. Luijten, Nano Lett. **6**, 901 (2006).
[22] M. Mihovilovic, N. Hagerty, and D. Stein, Phys. Rev. Lett. **110**, 028102 (2013).
[23] D. Gaunt and S. Colby, J. Stat. Phys. **58**, 539 (1990).
[24] B. Duplantier, J. Stat. Phys. **54**, 581 (1989).
[25] M. Rubenstein and R. H. Colby, *Polymer Physics* (Oxford University Press, Oxford, UK, 2003).
[26] D. R. Tree, A. Muralidhar, P. S. Doyle, and K. D. Dorfman, Macromolecules **46**, 8369 (2013).
[27] M. F. Maghrebi, Y. Kantor, and M. Kardar, Europhys. Lett. **96**, 66002 (2011).
[28] M. F. Maghrebi, Y. Kantor, and M. Kardar, Phys. Rev. E **86**, 061801 (2012).
[29] D. Frenkel and B. Smit, *Understanding Molecular Simulation: From Algorithms to Applications*, 2nd ed. (Academic Press, London, 2002), Chap. 7.